Enhanced Third-Harmonic Generation from a Metal/Semiconductor Core/Shell Hybrid Nanostructure

Omri Bar-Elli, Eran Grinvald, Noga Meir, Lior Neeman, and Dan Oron*

Department of Physics of Complex Systems, Weizmann Institute of Science, Rehovot 76100, Israel

ABSTRACT Nonlinear optical processes can be dramatically enhanced *via* the use of localized surface plasmon modes in metal nanoparticles. Here we show how more elaborate structures, based on shape-controlled Au/Cu_2O core/shell nanostructures, enable further enhancement of the nanoparticle third-harmonic scattering cross-section. The semiconducting component takes a twofold role in this structure, both providing a knob to tune the resonant frequency of the gold plasmon and providing resonant enhancement by virtue of its excitonic states. The advantages and deficiencies of using such core/shell metal/semiconductor structures are discussed.

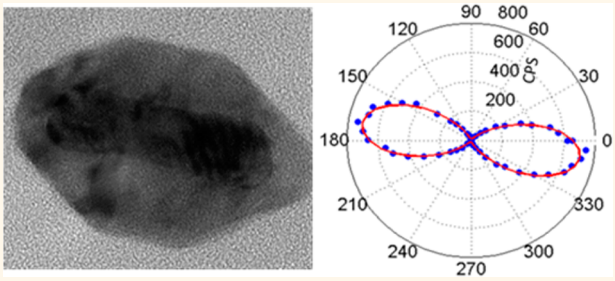

KEYWORDS: plasmonics · third-harmonic generation · core/shell nanoparticles

The use of metal nanoparticles as nanometric tags in bioimaging applications has grown dramatically over the last two decades. In particular, noble metal nanoparticles are characterized by strong shape-tunable plasmonic resonances, which lead to large absorption and scattering cross-sections, making them useful in numerous applications. Noble metal nanoparticles, particularly ones made from gold, have been found to be particularly useful in multiphoton microscopy. Despite their low emission quantum yields, the stability, absence of phototoxicity or blinking, and the ease of excitation have rendered gold nanospheres and gold nanorods attractive two-photon fluorescence (TPEF) markers.[1,2] To a lesser extent, metal particles have already seen application in nonlinear microscopies based on coherent scattering such as second-harmonic generation[3] (SHG) and third-harmonic generation (THG).[4−6] In contrast to TPEF, coherent methods enable the use of holographic detection for three-dimensional tracking of particles.[7] Moreover, the SHG or THG spectrum depends on that of the excitation pulse used and can thus be tailored to the properties of the sample. One of the major drawbacks of using coherent scattering is the different scaling of the signal with the nanoparticle size. Whereas absorption scales with the volume of the nanoparticle, scattering processes scale with the square of the volume, thus typically requiring significantly larger particles to observe a strong signal.

From symmetry considerations, SHG is only allowed (to lowest order) from non-centrosymmetric structures. Yet, despite the fact that bulk gold is, by itself, centrosymmetric, SHG has been observed from plasmon-resonant nanospheres and nanorods (attributed to imperfections in their surfaces) but is significantly enhanced when the overall shape is non-centrosymmetric. Nanoparticles from non-centrosymmetric materials such as ZnO or $BaTiO_3$ have proven much more useful in SHG imaging applications.[4,8−10] Using these, single particles having diameters down to about 30 nm can be readily observed. For some applications, further reduction in the nanoparticle size is required, whereas for others uptake of larger particles is beneficial.[11−14] One pathway for either reducing particle size or enhancing the scattering efficiency, which has already been applied in SHG, is the utilization of materials that are resonant at the harmonic frequency. Using semiconducting particles based on CdTe/CdS hybrids has indeed reduced the required volume of SHG-active nanoparticles by 1 to 2 orders of magnitude.[15,16]

* Address correspondence to dan.oron@weizmann.ac.il.

Received for review March 26, 2015 and accepted July 21, 2015.

Published online July 21, 2015
10.1021/acsnano.5b01834

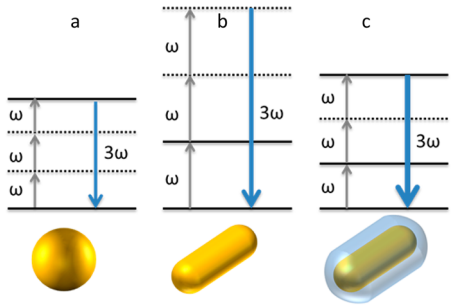

Figure 1. Enhancement schemes of THG using material resonances. Dashed lines are virtual states, and full lines are real levels. (a) Gold nanospheres show an LSPR mode at ~520 nm (3ω); making use of this resonance for enhancement requires excitation at ~1500 nm (ω).[17] (b) Gold nanorods exhibit two resonances, specifically a red-shifted longitudinal LSPR mode, allowing use of on-resonance illumination (ω = ~800 nm).[18] (c) Core/shell nanoparticles enable enhancement from both on-resonance illumination (longitudinal LSPR mode, ω = 1200 nm) and on-resonance THG signal (excitons, 3ω = 400 nm).

Unlike SHG, observation of THG imposes no symmetry restrictions on the particle shape or composition. THG from single gold nanospheres was demonstrated[17] using illumination such that the third-harmonic frequency was in resonance with the localized surface plasmon resonance (LSPR) of the nanospheres (Figure 1a). In this manner, it was possible to observe particles having a diameter as small as 40 nm with 1.5 μm infrared excitation. Significant enhancement[19] of the THG cross-section was measured using on-resonance illumination of the longitudinal LSPR mode of gold nanorods[18] (Figure 1b). Furthermore, the particles' rod geometry enabled detection of their orientation due to the strong polarization dependence of the nanorod THG signal. Yet, the excitation power in these experiments is significantly limited by reshaping of the nanorods, and the THG signal is typically in the UV range. Here we attempt to overcome both of these difficulties by constructing a hybrid core/shell metal/semiconductor THG scatterer. This shifts the fundamental frequency further to the near-infrared (due to dielectric effects) such that the THG is in the visible range and allows for doubly resonant THG, both at the fundamental and at the third-harmonic frequencies (due to resonant absorption in the semiconductor). As an added benefit, this may provide a pathway toward diminishing the size of THG markers.

Coating a metallic nanorod with a high refractive index material causes a red shift in the longitudinal LSPR mode according to ref 20 (assuming an ellipsoidal shape):

$$\omega^2 = \frac{L\omega_p^2}{\varepsilon_m - L(\varepsilon_m - 1)}$$

where ω is the LSPR resonance frequency, $0 < L < 1$ is the shape factor, which depends on the aspect ratio, ω_p is the material plasma frequency from the Drude model, and ε_m is the medium's dielectric constant. It was shown that certain wavelengths in the IR regime allow deeper penetration to biological tissue due to decreased absorption by water. Thus, a red shift in the LSPR makes core/shell nanoparticles better suited for applications in harmonic generation microscopy. In our proposed enhancement scheme (Figure 1c), the fundamental frequency is resonant with the longitudinal LSPR mode in the metallic core, while the THG is resonant with the excitonic transition of the semiconducting shell. In this scheme, the THG frequency is red-shifted from the UV to the visible without increasing the aspect ratio of the metal rod. Overall, this can allow for higher collection efficiencies and potentially deeper penetration into tissue. As a shell material, we chose cuprous oxide (Cu_2O), a semiconductor with a band gap of 2.14 eV, enabling resonant THG in a broad range of excitation wavelengths. Cu_2O nanoparticles[21−23] have found use in biological studies,[24] and their toxicity has been studied in different organisms and has been shown to be significantly lower than other semiconductors with a similar band gap such as CdSe.[25,26]

RESULTS AND DISCUSSION

The synthesis of cuprous oxide-coated gold nanorods (AuNR@Cu_2O) follows a known procedure.[27,28] Seeded growth of Au nanorods (AuNR) is performed using a binary mixture of surfactants;[29] then a reduction of Cu^{2+} by NH_2OH in the presence of the AuNR cores takes place in an aqueous solution, yielding an epitaxial shell around the AuNR. Control of the semiconductor shell thickness is achieved by tuning the Cu^{2+} concentration in the reaction vial[28] (see the Supporting Information).

Systematically increasing the Cu_2O shell thickness gradually increased the effective dielectric constant surrounding the AuNR cores, causing an increased red shift of the LSPR modes (Figure 2). Due to the relatively small Bohr radius[31] of excitons in Cu_2O (~7 Å), all shell thicknesses examined should exhibit a band gap similar to bulk Cu_2O (~2.14 eV). Yet, this is not clearly evident in the extinction spectra shown in Figure 2. We attribute the extinction dip at ~550 nm to strong coupling[30] between the transverse LSPR mode of the AuNR core and the Cu_2O shell band edge exciton. This assignment is supported by the observed red shift of the dip position as the Cu_2O shell thickness is increased, leading to a red shift of the transverse LSPR peak (Figure 2, curves b−d). Thus, at least for intermediate shell thicknesses, the extinction peak resonant with the THG wavelength partially retains LSPR properties, which may lead to enhanced light scattering. We chose to work with the sample portrayed in Figure 2c in the single-particle scattering experiments.

Single-particle measurements were conducted using a custom setup based around an inverted microscope

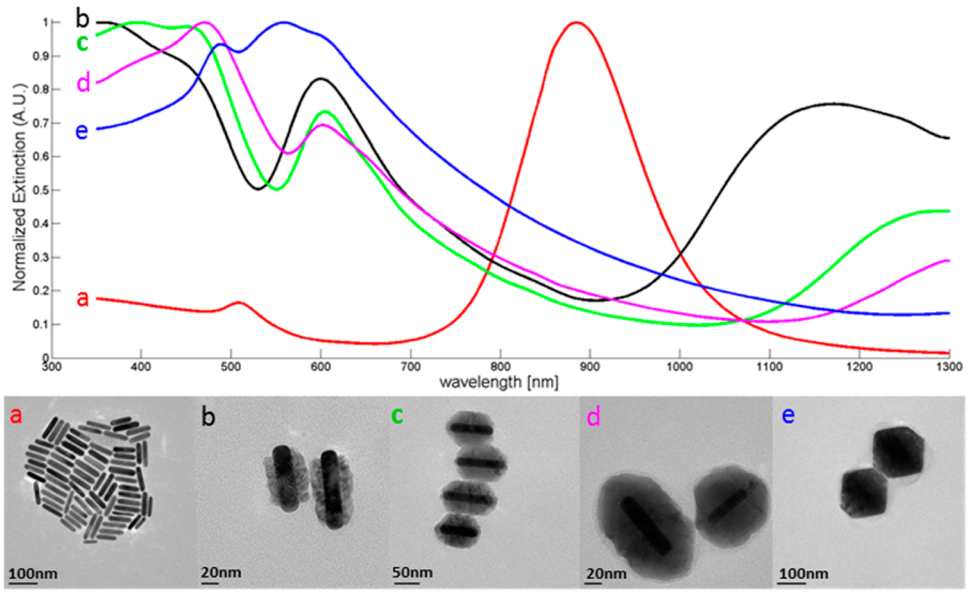

Figure 2. Extinction spectra and corresponding TEM images of AuNR and AuNR@Cu_2O samples with different Cu_2O shell thickness. The AuNR cores are visible through the Cu_2O shell due to the much higher electron density in the metal. Red shift of the longitudinal LSPR mode with increasing shell thickness is clearly visible in the spectra; the transverse LSPR mode appears to be strongly coupled to the excitonic states of the semiconductor shell, resulting in a characteristic dip in the extinction spectrum.[30]

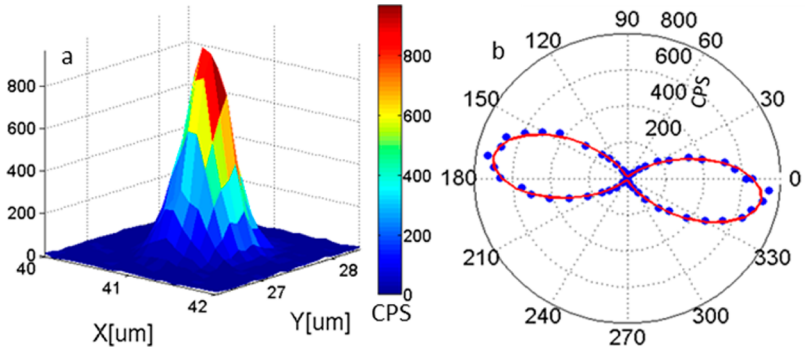

Figure 3. (a) Third-harmonic generation from a single AuNR@Cu_2O particle as a function of stage position (X,Y). Pixels are 100 × 100 nm. (b) Signal dependence on incident linear polarization. Fit (solid line) to the data (circles) is a third-order dipole response ($a\cos^6(a+\varphi)+b$).

and using an 80 MHz, 1200 nm femtosecond source and time-correlated single photon counting (see the Methods section). Figure 3a is a typical scan of a single AuNR@Cu_2O particle. A fit to a 2D Gaussian function is used to verify the object size is indeed diffraction limited. Another indication that the object is a single particle comes from measuring the signal dependence on the orientation of the incident linear polarization. The rod shape of the core gives rise to a dipole-like response to the incoming linearly polarized field. Figure 3b shows a measurement of the THG signal polarization dependence, and a fit to a third-order response ($a\cos^6(a+\varphi)+b$) is presented. We compare our results with previous work,[17,18] so as to estimate the effect of the semiconductor shell on the THG efficiency. A comparison of the parameters of the three systems discussed here (all schematically shown in Figure 1), gold spheres, bare AuNRs, and AuNR/Cu_2O core/shell particles, appears in Table 1. To adequately compare signal levels, we estimate the efficiency of the different collection systems by taking into account the NA of the collection objective, the detector efficiencies at the different signal wavelengths, the quality of the spectral filters, and the losses due to coupling into an optical fiber.

$$\text{efficiency} = \text{NA}^2 \times \text{filter efficiency} \times \text{detector efficiency} \times \text{fiber coupling losses}$$

Normalizing the results by the obtained efficiency factor and the cube of the power density [counts per second (CPS)/(efficiency × power density^3)] we calculate an over 10^6 enhancement of the THG signal over gold nanospheres.[17] The median enhancement over the highest reported value in bare rods is about 3, whereas the maximal enhancement observed for a single particle is about 50[18] (Table 1). We note that our epi-detected

TABLE 1. Comparison of the Cross-Section and Damage Threshold of AuNR@Cu_2O Nanoparticles to Gold Nanospheres and Nanorods[a]

material	Au spheres[17]	Au rods[18]	Au@Cu_2O
resonance scheme	3ω	ω	ω and 3ω
excitation wavelength (nm)	1500	800	1200
particle volume (nm^3)	5.2×10^5	4.5×10^4	core: 2.5×10^4 total: 3.2×10^5
excitation power (MW/cm^2)	0.54	0.13	0.017
maximal CPS	1000	7000	11 000
cross-section[b] [CPS/(collection efficicncy $\times$ power density^3)]	1.0	maximal: 1.4×10^6	median: 3.9×10^6 maximal: 6.1×10^7

[a] Taking into account that the shell is transparent to 1200 nm illumination, the enhancement in cross-section of the Au@Cu_2O is in fact larger than depicted in the table due to the smaller core volume used (the scattering process scales as the square of the volume). [b] Assuming linear polarization along the rod axis for nanorods.

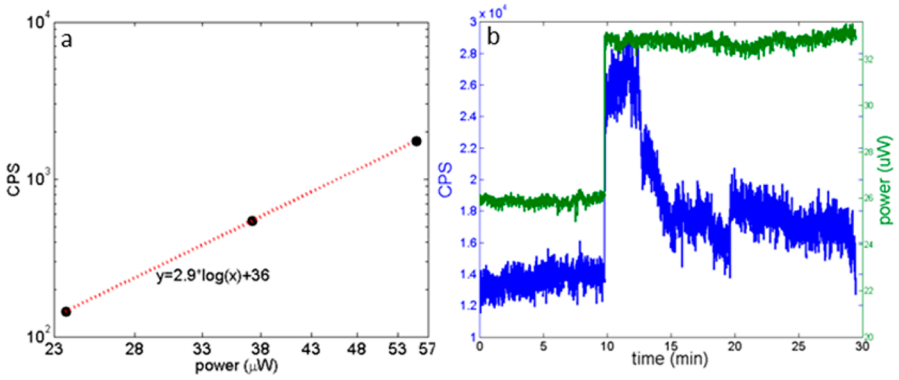

Figure 4. (a) Measurement showing the third-order power law of the signal at low excitation powers. (b) THG measurement from a single AuNR@Cu_2O over 30 min under continuous illumination, showing the stable signal below the damage threshold, and fluctuations in the signal right after increasing the power (t = 10 min) above the damage threshold. The signal cannot be regained, indicating permanent damage to the particle.

signal suffers from chromatic aberrations, which are more severe for near-infrared excitation. Given this, we estimate that the enhancement over bare AuNR is in fact even somewhat larger. As noted above, some particles exhibited higher THG enhancement than the average. This is likely due to the distribution of size and plasmon resonance wavelength within the nanoparticle ensemble (as seen in Figure 2).

Photothermal reshaping of the AuNR is the main damage mechanism found when working with intense femtosecond lasers (0.8 MW/cm^2) resonant with the particle LSPR.[18,32,33] To test for the damage threshold of the hybrid metal/semiconductor particles, we have conducted an experiment where excitation power is incrementally increased, while monitoring the THG signal. At low excitation powers the signal increases as the third power of the excitation intensity (Figure 4a). Above a certain power threshold, the signal begins to fluctuate for several minutes before reaching a new stable state with lower THG scattering efficiency. This transition is depicted (for a different particle) in Figure 4b, where stable THG is observed until the increase in laser power at t = 10 min. Following the increase in laser intensity, significant fluctuations in the signal intensity are observed, eventually leading to a new, relatively stable, signal state. In this new state, the signal is lower than what could be predicted by extrapolation of a third-order power law based on low power measurements. This indicates some irreversible damage to the scatterer. Unfortunately, the excitation power at which the core/shell structure exhibits this is much lower than for bare AuNRs. The damage threshold of hybrid structures varies among different particles, but is about 0.02 MW/cm^2 (Table 1). This indicates that the damage mechanism in the hybrid metal/semiconductor system is not reshaping of the metal core. Notably, the damage threshold of the particles is orders of magnitude lower than the biological damage threshold at 1.2 μm.[34]

To further elucidate the physical origin of the observed photodamage process of the core/shell particles, a 5 ns pulsed laser @1200 nm with a 10 Hz repetition rate was used to illuminate a solution of AuNR@Cu_2O while the extinction spectrum of the solution was monitored (Figure 5). The pulse energy was tuned so as to be just above the damage threshold discussed above. A uniform decrease of the entire extinction spectrum with time was observed. TEM images of samples taken at several time intervals (Figure 5) revealed that the Cu_2O fragments and disintegrates, leaving bare, intact, AuNR cores. Cu_2O fragments were not found in the TEM images. This led us to believe that the damage occurs

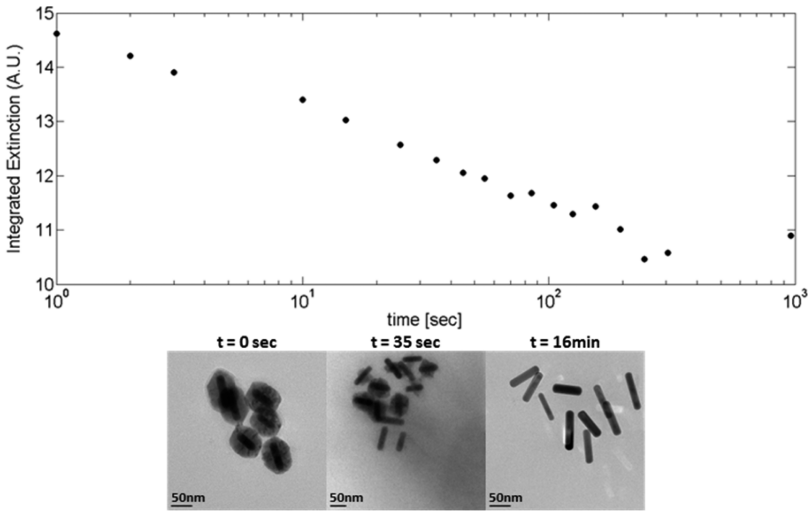

Figure 5. Extinction decrease from a solution of AuNR@Cu_2O nanoparticles while illuminating with 1200 nm pulses with a 10 Hz repetition rate and power density above the damage threshold. TEM pictures show the Cu_2O shell breaking and leaving the AuNR cores intact. After 4–5 min there is no more reaction to the laser illumination, but the extinction does not decrease to zero. This indicates that some of the particles would not undergo damage at this specific power level.

at the core/shell interface. The most plausible mechanism for this is thermal expansion. The thermal expansion coefficient of gold is almost 10 times larger than that of Cu_2O (14.5×10^{-6} and 1.6×10^{-6} K^{-1}, respectively).[35,36] This difference must cause strain between the core and the shell upon each illumination cycle, eventually leading to the shell's fracture and breakdown. This would explain the occurrence of irreversible damage after long exposure even at low power levels.

It should be noted that photodamage to the nanoparticles occurs on a time scale of minutes, as is evident from Figure 4b. To quantify the effect under practical imaging conditions, we conducted a set of experiments where the field of view containing the nanoparticles was repeatedly scanned every 3 min at an excitation power of approximately 4 times the damage threshold and with a pixel dwell time of 100 ms. Under these conditions, the scattering signal was thousands of counts per second for over 12 h (see the Supporting Information), showing the practical utility of these particles for prolonged imaging.

We expect that changing the particle's composition, such that the thermal expansion coefficient of the two materials would be better matched, may significantly increase the damage threshold and stability of the structure under intense illumination. One such potential system is a cobalt monoxide-coated gold nanorod (AuNR@CoO); CoO has a thermal expansion coefficient similar to gold[37] (14×10^{-6} K^{-1}) and a band gap of 2.4 eV, fulfilling the criteria for both resonant enhancement of the THG process and thermal stability. Another pathway to increase the photostability of the nanostructure may be to grow another shell on top of the semiconductor, composed of a more rigid material such as silica. This may also contribute to the biocompatibility of such structures.

CONCLUSIONS

In conclusion, we measured enhancement by a factor of about an order of magnitude of the THG cross-section from AuNR@Cu_2O hybrid structures over bare AuNR cores due to the new resonance scheme. Even though the damage threshold of our core/shell particles is lower than expected, we were still able to measure a stable and strong scattering signal at a level of several thousands of counts per second. The experimental observations provide guidance toward the design of core/shell THG scatterophores with increased damage thresholds.

METHODS

Synthesis. The synthesis of gold nanorods follows known procedures. Seeds were prepared by reducing a solution of $HAuCl_4$ with $NaBH_4$ using cetyl trimethylammonium bromide (CTAB) as a surface agent. To grow the AuNR, CTAB and NaOL were used as surfactants, $AgNO_3$ and HCl were used to tune the final AuNR size, and ascorbic acid was used to reduce the $HAuCl_4$ in the solution. The cuprous oxide (Cu_2O) shell was grown in a solution containing 87 mg of sodium dodecyl sulfate (SDS) in water. A 0.25 mL amount of 1 M NaOH was used to increase the pH such that the resulting Cu_2O was stable in solution. A 2 μmol (typically) portion of $CuCl_2$ was reduced by a large excess of $NH_2OH \cdot HCl$ in the presence of the AuNR to form a shell of Cu_2O. Control over the shell's thickness was achieved by changing the $CuCl_2$ concentration (see Supporting Information).

Single-particle THG measurements: 100 fs pulses at 800 nm at an 80 MHz repetition rate from a Ti:sapphire laser (Coherent, Chameleon Ultra II) were downconverted using a synchronously pumped optical parametric oscillator (OPO) (Coherent, Chameleon Compact OPO), to get the 1200 nm laser wavelength desired for excitation. The laser was directed into a microscope (Zeiss Axiovert

200 inverted microscope) and focused using an oil immersion objective (Zeiss Plan Apochromat X63 NA 1.4). The spectrally filtered signal was epi-detected, coupled to a multimode fiber, and detected by a single-photon avalanche photodiode (Laser Components, Count Blue) that was connected to a time-correlated single-photon counting system (Picoquant HydraHarp 400). Samples were prepared using microscope coverslips with an adhesion layer of (3-mercaptopropyl)trimethoxysilane (see Supporting Information).

Conflict of Interest: The authors declare no competing financial interest.

Supporting Information Available: Detailed synthesis of AuNR@Cu_2O nanoparticles and sample preparation method. Video depicting the effect of photodamage of a single particle in practical imaging conditions. The Supporting Information is available free of charge on the ACS Publications website at DOI: 10.1021/acsnano.5b01834.

Acknowledgment. The authors acknowledge financial support by the Minerva Foundation, the Israeli Centers of Research Excellence Program, the European Research Council Starting Investigator Grant SINSLIM 258221, and the Crown Photonics Center.

REFERENCES AND NOTES

1. Huff, T. B.; Hansen, M. N.; Zhao, Y.; Cheng, J.; Wei, A. Controlling the Cellular Uptake of Gold Nanorods. *Langmuir* **2007**, *23*, 1596–1599.
2. Durr, N. J.; Larson, T.; Smith, D. K.; Korgel, B. a.; Sokolov, K.; Ben-Yakar, A. Two-Photon Luminescence Imaging of Cancer Cells Using Molecularly Targeted Gold Nanorods. *Nano Lett.* **2007**, *7*, 941–945.
3. Butet, J.; Duboisset, J.; Bachelier, G.; Russier-Antoine, I.; Benichou, E.; Jonin, C.; Brevet, P. F. Optical Second Harmonic Generation of Single Metallic Nanoparticles Embedded in a Homogeneous Medium. *Nano Lett.* **2010**, *10*, 1717–1721.
4. Cohen, B. E. Biological Imaging: Beyond Fluorescence. *Nature* **2010**, *467*, 407–408.
5. Yelin, D.; Oron, D.; Thiberge, S.; Moses, E.; Silberberg, Y. Multiphoton Plasmon-Resonance Microscopy. *Opt. Express* **2003**, *11*, 1385–1391.
6. Yelin, D.; Silberberg, Y. Laser Scanning Third-Harmonic-Generation Microscopy in Biology. *Opt. Express* **1999**, *5*, 169–175.
7. Hsieh, C.-L.; Grange, R.; Pu, Y.; Psaltis, D. Three-Dimensional Harmonic Holographic Microcopy Using Nanoparticles as Probes for Cell Imaging. *Opt. Express* **2009**, *17*, 2880–2891.
8. Pu, Y.; Grange, R.; Hsieh, C.-L.; Psaltis, D. Nonlinear Optical Properties of Core-Shell Nanocavities for Enhanced Second-Harmonic Generation. *Phys. Rev. Lett.* **2010**, *104*, 1–4.
9. Staedler, D.; Magouroux, T.; Hadji, R.; Joulaud, C.; Extermann, J.; Schwung, S.; Passemard, S.; Kasparian, C.; Clarke, G.; Gerrmann, M.; et al. Harmonic Nanocrystals for Biolabeling: A Survey of Optical Properties and Biocompatibility. *ACS Nano* **2012**, *6*, 2542–2549.
10. Pantazis, P.; Maloney, J.; Wu, D.; Fraser, S. E. Second Harmonic Generating (SHG) Nanoprobes for *in Vivo* Imaging. *Proc. Natl. Acad. Sci. U. S. A.* **2010**, *107*, 14535–14540.
11. Sharma, P.; Brown, S.; Walter, G.; Santra, S.; Moudgil, B. Nanoparticles for Bioimaging. *Adv. Colloid Interface Sci.* **2006**, *123−126*, 471–485.
12. Jiang, Y.; Horimoto, N. N.; Imura, K.; Okamoto, H.; Matsui, K.; Shigemoto, R. Bioimaging with Two-Photon-Induced Luminescence from Triangular Nanoplates and Nanoparticle Aggregates of Gold. *Adv. Mater.* **2009**, *21*, 2309–2313.
13. Hutter, E.; Maysinger, D. Gold Nanoparticles and Quantum Dots for Bioimaging. *Microsc. Res. Tech.* **2011**, *74*, 592–604.
14. Hilderbrand, S. a; Shao, F.; Salthouse, C.; Mahmood, U.; Weissleder, R. Upconverting Luminescent Nanomaterials: Application to *in Vivo* Bioimaging. *Chem. Commun. (Cambridge, U. K.)* **2009**, 4188–4190.
15. Winter, S.; Zielinski, M.; Chauvat, D.; Zyss, J.; Oron, D. The Second Order Nonlinear Susceptibility of Quantum Confined Semiconductors—A Single Dot Study. *J. Phys. Chem. C* **2011**, *115*, 4558–4563.
16. Zielinski, M.; Oron, D.; Chauvat, D.; Zyss, J. Second-Harmonic Generation from a Single Core/shell Quantum Dot. *Small* **2009**, *5*, 2835–2840.
17. Lippitz, M.; Van Dijk, M. A.; Orrit, M. Third-Harmonic Generation from Single Gold Nanoparticles. *Nano Lett.* **2005**, *5*, 799–802.
18. Schwartz, O.; Oron, D. Background-Free Third Harmonic Imaging of Gold Nanorods. *Nano Lett.* **2009**, *9*, 4093–4097.
19. Boyd, R. W. *Nonlinear Optics*; Academic Press: London, UK, 2003.
20. Bohren, C.; Huffman, D. *Absorption and Scattering of Light by Small Particles*; Wiley-VCH Verlag GmbH: Weinheim, Germany, 1983.
21. Fan, W.; Shi, Z.; Yang, X.; Cui, M.; Wang, X.; Zhang, D.; Liu, H.; Guo, L. Bioaccumulation and Biomarker Responses of Cubic and Octahedral Cu2O Micro/nanocrystals in Daphnia Magna. *Water Res.* **2012**, *46*, 5981–5988.
22. Lanone, S.; Rogerieux, F.; Geys, J.; Dupont, A.; Maillot-Marechal, E.; Boczkowski, J.; Lacroix, G.; Hoet, P. Comparative Toxicity of 24 Manufactured Nanoparticles in Human Alveolar Epithelial and Macrophage Cell Lines. *Part. Fibre Toxicol.* **2009**, *6*, 14.
23. Chen, L. Q.; Kang, B.; Ling, J. Cytotoxicity of Cuprous Oxide Nanoparticles to Fish Blood Cells: Hemolysis and Internalization. *J. Nanopart. Res.* **2013**, *15*.10.1007/s11051-013-1507-7
24. Qi, W. J.; Huang, C. Z.; Chen, L. Q. Cuprous Oxide Nanospheres as Probes for Light Scattering Imaging Analysis of Live Cells and for Conformation Identification of Proteins. *Talanta* **2010**, *80*, 1400–1405.
25. Derfus, A. M.; Chan, W. C. W.; Bhatia, S. N. Probing the Cytotoxicity of Semiconductor Quantum Dots. *Nano Lett.* **2004**, *4*, 11–18.
26. Pace, H. E.; Lesher, E. K.; Ranville, J. F. Influence of Stability on the Acute Toxicity of CdSe/ZnS Nanocrystals to Daphnia magna. *Environ. Toxicol. Chem.* **2010**, *29*, 1338–1344.
27. Kuo, C. H.; Hua, T. E.; Huang, M. H. Au Nanocrystal-Directed Growth of Au - Cu2O Core - Shell Heterostructures with Precise Morphological Control. *J. Am. Chem. Soc.* **2009**, *131*, 17871–17878.
28. Meir, N.; Jen-La Plante, I.; Flomin, K.; Chockler, E.; Moshofsky, B.; Diab, M.; Volokh, M.; Mokari, T. Studying the Chemical, Optical and Catalytic Properties of Noble Metal (Pt, Pd, Ag, Au)−Cu 2 O Core−shell Nanostructures Grown *via* a General Approach. *J. Mater. Chem. A* **2013**, *1*, 1763.
29. Ye, X.; Zheng, C.; Chen, J.; Gao, Y.; Murray, C. B. Using Binary Surfactant Mixtures To Simultaneously Improve the Dimensional Tunability and Monodispersity in the Seeded Growth of Gold Nanorods. *Nano Lett.* **2013**, *13*, 765–771.
30. Zengin, G.; Johansson, G.; Johansson, P.; Antosiewicz, T. J.; Käll, M.; Shegai, T. Approaching the Strong Coupling Limit in Single Plasmonic Nanorods Interacting with J-Aggregates. *Sci. Rep.* **2013**, *3*, 3074.
31. Fishman, D. *Excitons in Cuprous Oxide*; University of Groningen, 2008.
32. Link, S.; Burda, C.; Nikoobakht, B.; El-Sayed, M. A. Laser-Induced Shape Changes of Colloidal Gold Nanorods Using Femtosecond and Nanosecond Laser Pulses. *J. Phys. Chem. B* **2000**, *104*, 6152–6163.
33. Link, S.; Burda, C.; Mohamed, M. B.; Nikoobakht, B.; El-Sayed, M. A. Laser Photothermal Melting and Fragmentation of Gold Nanorods: Energy and Laser Pulse-Width Dependence. *J. Phys. Chem. A* **1999**, *103*, 1165–1170.
34. Supatto, W.; Débarre, D.; Farge, E.; Beaurepaire, E. Femtosecond Pulse-Induced Microprocessing of Live Drosophila Embryos. *Med. Laser Appl.* **2005**, *20*, 207–216.
35. Tiano, W.; Dapiaggi, M.; Artioli, G. Thermal Expansion in Cuprite-Type Structures from 10 K to Decomposition Temperature: Cu2O and Ag2O. *J. Appl. Crystallogr.* **2003**, *36*, 1461–1463.
36. Solliard, C.; Flueli, M. Surfaces Stress and Size Effect on the Lattice Parameter in Small Particles of Gold and Platinum. *Surf. Sci. Lett.* **1985**, *156*, A321.
37. Samsonov, G. V. *The Oxide Handbook*, 2nd ed.; IFI/Plenum: New York, 1982.